Dynamic Shear Strength of GMX/GCL Composite Liner for Monotonic Loading

Jason D. Ross, M.ASCE[1]; and Patrick J. Fox, F.ASCE[2]

Abstract: This paper presents an experimental investigation of the dynamic shear strength of a composite liner consisting of a high-density polyethylene (HDPE) textured geomembrane (GMX) over a hydrated nonwoven/nonwoven needle-punched geosynthetic clay liner (GCL) for monotonic (i.e., single direction) loading conditions. Displacement-controlled shear tests were conducted using a large direct shear machine for five normal stress levels ranging from 13 to 2071 kPa and five shear displacement rates ranging from 0.1 to 30,000 mm/min. GCL internal failures occurred at high normal stress and low displacement rate. As normal stress decreased or displacement rate increased, failure mode transitioned to the GMX/GCL interface. Peak strength envelopes are slightly nonlinear (concave-down) and show dependence on displacement rate at higher normal stress. Large-displacement strength envelopes show greater dependence on displacement rate at higher normal stress due to the effect of changing failure mode. The standard displacement rate for static shear tests of GMX/GCL composite liners (1 mm/min) yielded conservative values of peak shear strength but unconservative values of large-displacement shear strength for some normal stress conditions. The GMX/GCL composite liner experienced significant post-peak strength reduction for all test conditions. **DOI: 10.1061/(ASCE)GT.1943-5606.0001198.**

Author keywords: Geomembrane; Geosynthetic clay liner; Composite liner; Bentonite; Shear strength; Direct shear; Displacement rate.

Introduction

Textured geomembranes (GMXs) are commonly placed over geosynthetic clay liners (GCLs) in the construction of composite liners for landfills and other waste containment facilities. The shear strength of a GMX/GCL composite liner warrants particular attention because bentonite, the essential component of a GCL, is a weak material after hydration and can provide a potential surface for instability. Hydrated bentonite yields low residual strength if a GCL fails internally and also can migrate through the geotextiles of a GCL to reduce interface shear strength with an adjacent geomembrane. Extensive research has been conducted on GMX/GCL interface shear strength for static loading conditions (Gilbert et al. 1996; Stark and Eid 1996; Daniel et al. 1998; Triplett and Fox 2001; Chiu and Fox 2004; Fox and Kim 2008; Vukelic et al. 2008; McCartney et al. 2009; Chen et al. 2010; Eid 2011; Fox and Ross 2011; Thielmann et al. 2013), and data are available on dynamic (e.g., monotonic, cyclic) internal shear strength for GCLs (Lai et al. 1998; Nye and Fox 2007; Fox et al. 2015). In addition, three studies have been conducted using shake tables to investigate the cyclic shear strength of smooth geomembrane/GCL interfaces under low normal stress (Lo Grasso et al. 2002; Park et al. 2004; Kim et al. 2005). However, no previous studies have been conducted on the dynamic shear strength of GMX/GCL composite liners. This information is important for dynamic loading applications, such as the design and long-term performance assessment of facilities that contain GCLs in seismic regions.

Limited information is available on the effect of shear displacement rate for GMX/GCL interface shear strength. Triplett and Fox (2001) found that displacement rate had no effect, on average, for peak and large-displacement interface strengths between the woven side of a woven/nonwoven (W/NW) needle-punched (NP) GCL and two types of high-density polyethylene (HDPE) GMX for normal stress $\sigma_n = 72$ kPa and displacement rate $R = 0.01$–10 mm/min. This is in agreement with the findings of Stark et al. (1996), in which displacement rate did not significantly affect peak and residual strengths for a GMX/NW geotextile (GT) interface ($\sigma_n = 96$ kPa; $R = 0.029$–36.7 mm/min). McCartney et al. (2002, 2009) also reported that displacement rate had little effect on interface shear strength between GCLs and various textured geomembranes ($\sigma_n \leq 345$ kPa; $R = 0.025$–1 mm/min). The above studies were conducted for low to intermediate normal stress levels ($\sigma_n \leq 345$ kPa) and with displacement rates in the quasi-static range ($R \leq 36.7$ mm/min). Based on these findings, Fox and Stark (2004) recommended a displacement rate of 1 mm/min for static shear tests of hydrated GMX/NP GCL interfaces.

The location of a potential failure surface within a GMX/GCL composite liner is controlled by internal peak shear strength of the GCL and interface peak shear strength between the GMX and GCL. Interface sliding is more likely to occur at low normal stress as indicated by failures of the Cincinnati test plots (Daniel et al. 1998) and results from static shear tests (e.g., Triplett and Fox 2001; McCartney et al. 2009). As normal stress increases, GCL internal strength may become limiting and cause the failure surface to move into the GCL. Although early studies reported such failure mode transitions at low normal stress (Byrne 1994; Gilbert et al. 1996), two recent studies on GMX/GCL composite liners have documented failure mode transition for $\sigma_n = 250$–300 kPa (Eid 2011) and $\sigma_n = 692$–$2{,}071$ kPa (Fox and Ross 2011). Thus, static shear tests have indicated: (1) contemporary GCLs have larger shear strengths than GMX/GCL interfaces in most cases; (2) GMX/

[1]Project Engineer, S&ME, Inc., Dublin, OH 43016. E-mail: jdross@smeinc.com

[2]Professor, Dept. of Structural Engineering, Univ. of California, San Diego, La Jolla, CA 92093-0085 (corresponding author). E-mail: pjfox@ucsd.edu

Note. This manuscript was submitted on September 10, 2013; approved on January 9, 2015; published online on February 26, 2015. Discussion period open until July 26, 2015; separate discussions must be submitted for individual papers. This paper is part of the ***Journal of Geotechnical and Geoenvironmental Engineering***, © ASCE, ISSN 1090-0241/04015026(11)/$25.00.

GCL liners can experience GCL internal failure if the normal stress is sufficiently high; and (3) the normal stress at failure mode transition can vary widely, depending on specific materials and test conditions. Static shear tests have also indicated that, for a given normal stress, hydrated GMX/GCL interfaces can be expected to have higher large-displacement shear strengths than internal failures of hydrated GCLs (Fox and Ross 2011).

This paper presents an experimental investigation of the dynamic shear strength of a composite liner consisting of a HDPE GMX over a hydrated NW/NW NP GCL for monotonic (i.e., single-direction) loading conditions. Displacement-controlled shear tests were conducted using a large direct shear machine for a wide range of normal stress levels and shear displacement rates. The data provide insight with regard to stress-displacement and volume change behavior, as well as variation of failure mode and peak and large-displacement shear strengths with normal stress and displacement rate. Some of the preliminary results were discussed by Ross et al. (2010). A companion paper (Fox et al. 2015) presents corresponding data for internal shear tests of a hydrated W/NW NP GCL. Shear strength information presented in these papers may be useful for preliminary design purposes; however, final design values must always be obtained from project-specific tests.

Experimental Program

GCL and GMX Materials

The experimental program was conducted using two common geosynthetic products, with specimens taken from the same shipments of material as used for the Fox and Ross (2011) static shear tests. The GCL was Bentomat DN, a NW/NW NP product with no thermal bonding manufactured by CETCO (Hoffman Estates, Illinois). This GCL contains granular bentonite held between two NW polypropylene geotextiles (200 g/m^2). The bentonite has a minimum dry mass/area of 3.7 kg/m^2 and a minimum free swell of 24 mL/2 g. To provide reinforcement, polypropylene fibers from the cover geotextile are needle-punched through the bentonite and carrier geotextile. The average peel strength of the GCL, as obtained from 25 wide-width tests (ASTM D6496), was 2,170 N/m, and the coefficient of variation (standard deviation/mean) of peel strength was 11%. The GMX was Micro Spike/Smooth, a HDPE product manufactured by Agru America (Georgetown, South Carolina) using a flat die extrusion calendaring process. This GMX has a thickness of 1.5 mm (60 mils), structured texturing on one side, and material properties given in Table 1. The average asperity (i.e., spike) height, as obtained from 25 measurements, was 0.72 mm (29 mils) and the coefficient of variation of asperity height was 18%. The manufacturer's specified minimum average asperity height for this product is 0.41 mm (16 mils). The average asperity spacing, as measured across 50 asperities (five measurements each direction), was 5.29 mm in the machine direction and 5.53 mm in the transverse direction (Ross 2009).

Table 1. Material Properties for HDPE GMX

Property	Method	Units	Values
Minimum/maximum/ average thickness	ASTM D5994 (ASTM 2010b)	mm	1.45/1.58/1.53
Density	ASTM D792 (ASTM 2013d)	g/cm^3	0.945
Tensile strength at yield/break	ASTM D6693 (ASTM 2010a)	N/mm	27/38
Tensile elongation at yield/break	ASTM D6693 (ASTM 2010a)	%	15.7/549
Dimensional stability	ASTM D1204 (ASTM 2014)	%	−0.78
Tear resistance	ASTM D1004 (ASTM 2013c)	N	243
Puncture resistance	ASTM D4833 (ASTM 2013b)	N	581

Equipment

All tests were conducted using the large dynamic direct shear machine described by Fox et al. (2006). A brief overview of machine design and operation are provided in the companion paper (Fox et al. 2015). For the current testing program, firm gripping surfaces were used to minimize slippage of the GMX/GCL composite liner specimens during shear. The floor of the test chamber was covered with modified truss plates to grip and permit free drainage for the GCLs. The smooth side of each GMX specimen was glued to the underside of the pullout plate using a water-resistant epoxy, and the ends were marked on the plate to detect slippage. If slippage occurred during shear, the test was rejected. These gripping surfaces permit a GMX/GCL specimen to fail along the weakest surface, including GCL internal failure, and reduce progressive failure effects associated with specimen slippage. Progressive failure has been shown to introduce significant distortion to GMX/GCL shear stress-displacement relationships, causing a reduction in peak strength, an increase in displacement at peak strength, and an increase in large-displacement, but not residual, shear strength (Fox and Kim 2008).

Procedures

GMX and GCL specimens were cut parallel to the machine direction of each product. GMX specimens had a length of 1,327 mm to allow additional material to move into the test chamber and thus maintain constant area of the failure surface during shear. The carrier geotextile for the GCL specimens also had a length of 1,327 mm, in case GCL internal failure occurred for a test. GCLs were hydrated using the two-stage accelerated procedure described by Fox et al. (1998) and Fox and Stark (2004). For the first stage of hydration, a GCL specimen was placed in a shallow pan and, depending on the normal stress level, the appropriate amount of tap water was added to bring the specimen to the estimated final water content for the test. The specimen was covered to minimize evaporation and allowed to cure for two days under low normal stress (1 kPa). For the second stage of hydration, the GCL was placed in the test chamber with the carrier geotextile facing upward. The pullout plate with a glued GMX specimen was placed on the GCL, the normal stress was applied, and the GCL was hydrated for an additional one to two days with free access to water. Similar to previous results (Fox et al. 1998, 2006; Triplett and Fox 2001; Fox and Ross 2011), most GCL specimens reached constant volume within 6 h using this procedure.

A total of 29 displacement-controlled monotonic shear tests were conducted to a final displacement of 200 mm for five normal stress levels (σ_n = 13, 348, 692, 1,382, and 2,071 kPa) and five displacement rates (R = 0.1, 1, 100, 10,000 mm/min, and R_{max}). Displacement rates of 0.1 and 1 mm/min are the recommended values for static internal shear tests of hydrated GCL and static interface shear tests of hydrated GMX/GCL specimens, respectively [ASTM D6243 (ASTM 2013a)]. The maximum displacement rate R_{max} was dependent on the required shear load and ranged from 30,000 mm/min at low normal stress to 20,000 mm/min at high normal stress. This range is more than three orders of magnitude higher than the highest displacement rates used in previous investigations (Triplett and Fox 2001; McCartney et al. 2009) and

Table 2. Summary of Experimental Program and Results

Normal stress σ_n (kPa)	Displacement rate R (mm/min)	Failure mode (internal/interface) (%)	Peak shear strength τ_p (kPa)	Displacement at peak shear strength δ_p (mm)	Large-displacement shear strength τ_{200} (kPa)	Final GCL water content	
						Mean (%)	Coefficient of variation (%)
13	1	0/100	7.9	3.8	6.1	231.0	9.2
13	100	0/100	8.9	2.7	5.6	223.2	23.3
13	10,000	0/100	14.2	3.9	5.7	215.1	15.4
13	30,000	0/100	14.7	4.3	5.9	223.8	14.0
348	0.1	0/100	124.2	12.7	73.2	81.7	12.3
348	1	0/100	124.3	12.4	70.7	87.6	14.2
348	100	0/100	122.5	11.4	61.3	91.2	19.5
348	10,000	0/100	122.4	8.4	60.8	97.7	7.9
348	27,000	0/100	126.5	6.2	64.9	98.8	16.0
692	0.1	0/100	239.0	13.0	134.9	67.3	13.7
692	1	0/100	218.3	12.4	106.3	67.1	15.2
692	100	30/70	243.6	13.5	81.4	78.1	18.6
692	100	0/100	240.5	14.9	84.7	69.5	17.6
692	10,000	0/100	212.4	10.6	97.8	74.7	8.6
692	25,000	0/100	229.8	3.6	122.2	80.5	18.4
1,382	0.1	20/80	425.0	15.5	170.8	46.7	16.1
1,382	1	80/20	394.9	15.5	107.2	56.3	7.4
1,382	1	100/0	401.9	16.2	96.9	50.9	13.0
1,382	100	30/70	425.3	13.3	126.7	47.8	8.0
1,382	100	20/80	431.7	14.9	120.5	53.0	11.8
1,382	10,000	100/0	436.3	10.8	166.3	65.1	21.0
1,382	23,000	0/100	442.7	4.1	165.8	50.8	27.8
1,382	23,000	0/100	460.8	5.1	—	65.5	12.2
2,071	0.1	100/0	550.1	16.7	164.0	37.3	12.5
2,071	1	100/0	568.4	16.7	136.5	40.4	15.3
2,071	1	100/0	515.6	16.7	136.3	43.4	6.4
2,071	100	20/80	652.9	15.4	188.5	43.2	6.4
2,071	10,000	0/100	615.2	13.2	215.5	48.3	7.7
2,071	20,000	0/100	618.3	5.3	230.7	42.3	6.8

produced complete shear failure in 0.4–0.6 s. After each test was completed, the GMX and GCL specimens were immediately removed from the machine and five water content measurements were taken from the GCL. The mode of failure was noted, including relative percentages of GCL internal and GMX/GCL interface shear and any other indications of localized distress to the geosynthetics (Ross 2009).

Results

Failure Mode and Final GCL Water Content

A summary of the experimental program and results is presented in Table 2. Depending on the normal stress and displacement rate, three failure modes were observed for the GMX/GCL specimens: GMX/GCL interface failure, GCL partial internal failure, and GCL internal failure. Interface failures occurred when the GMX sheared across the top of the GCL. This failure mode produced grooves in the upper geotextile but caused no serious damage to the GCL. For interface failures, final roughness of the GMX in the direction of shear, as determined manually, decreased with increasing normal stress due to flattening (i.e., bending) of the asperities. Partial internal failures occurred when the reinforcement failed over one or more areas of the GCL. Reinforcement failure resulted from pullout or rupture of the needle-punched fibers. The upper geotextile was easily separated from the lower geotextile and often displayed wrinkles, tears, or overlaps in these areas. Internal failures occurred when the reinforcement failed over the entire GCL. Similar to previous static shear tests (Fox and Ross 2011), such failures occurred at or just inside the upper (carrier) geotextile/bentonite interface and were uniform with little to no indications of localized distress to the geotextiles. Bentonite extrusion through the nonwoven geotextiles and around the edges of the specimens was insignificant.

Final GCL water contents, representing the average of five measurements for each GCL specimen (including geotextiles), are presented in Fig. 1 along with regression relationships. Values decrease with increasing normal stress and display good consistency at each stress level. For $\sigma_n = 13$ kPa, water contents decrease slightly with increasing displacement rate, whereas for

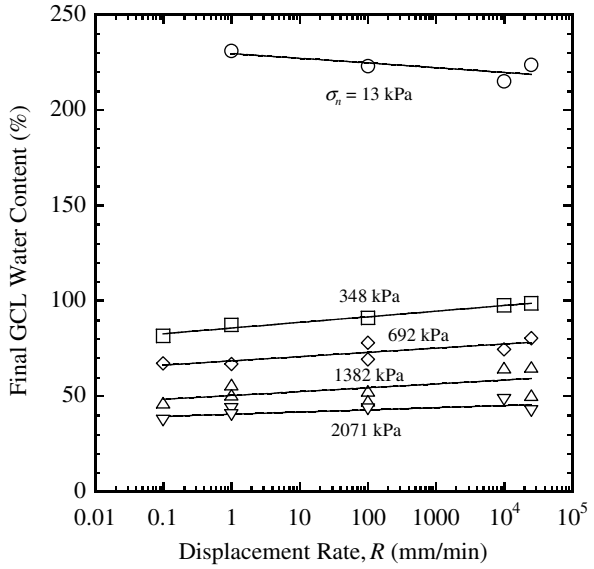

Fig. 1. Final GCL water contents

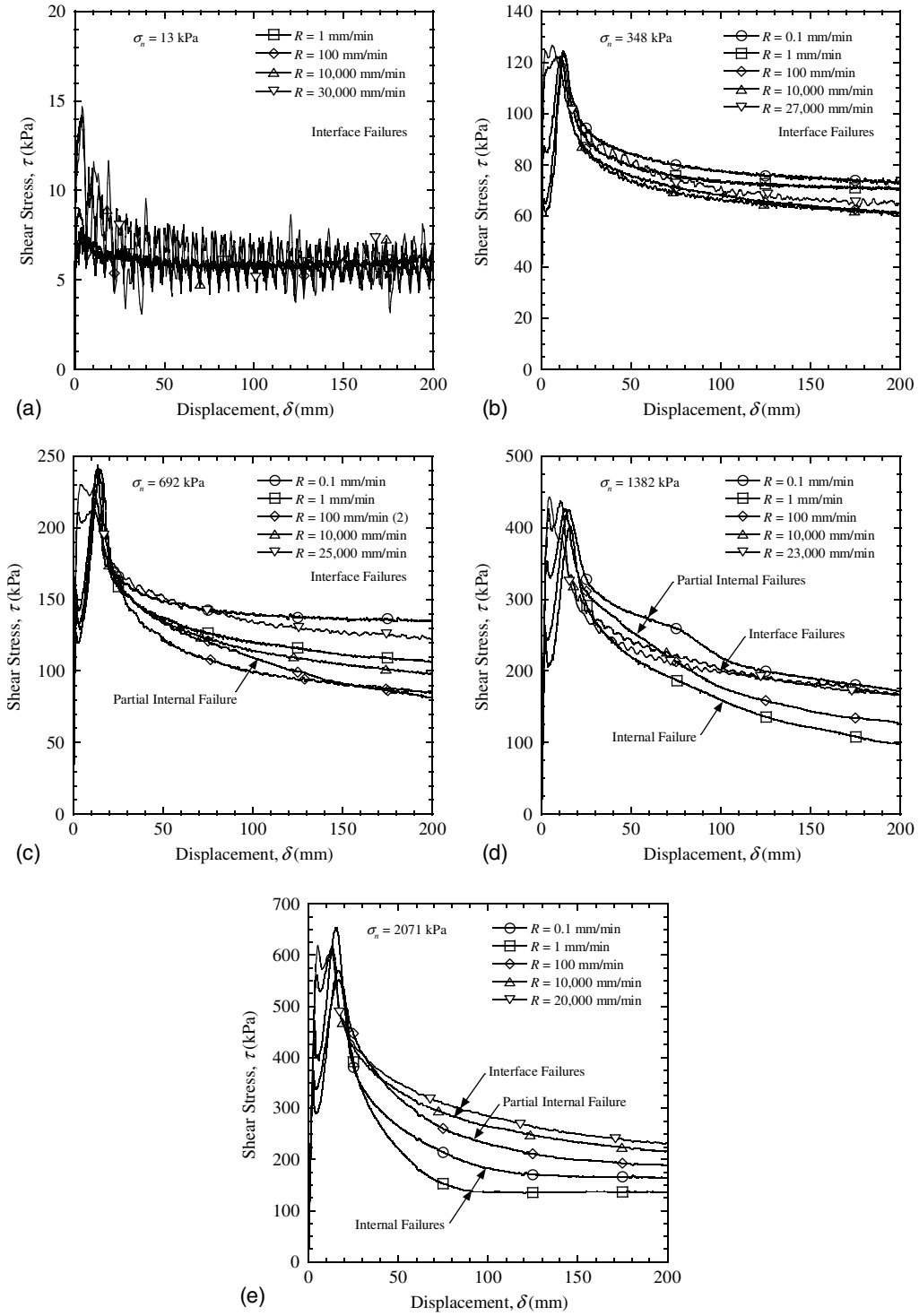

Fig. 2. Representative shear stress-displacement relationships: (a) $\sigma_n = 13$ kPa; (b) $\sigma_n = 348$ kPa; (c) $\sigma_n = 692$ kPa; (d) $\sigma_n = 1{,}382$ kPa; (e) $\sigma_n = 2{,}071$ kPa

$\sigma_n \geq 348$ kPa, the data show a reverse trend. Average values of coefficient of variation for the five measurements for each GCL specimen are 15.4, 12.9, 13.4, 13.7, and 13.9% for $\sigma_n = 13{,}348$, 692, 1,382, and 2,071 kPa, respectively, and are higher than corresponding values for the GCL internal shear tests (Fox et al. 2015).

Stress-Displacement Behavior

Representative relationships for shear stress τ versus shear displacement δ at five normal stress levels are presented in Fig. 2. Measured values of shear stress were corrected for inertia force of the pullout plate and applicable actuator components. The relationships display generally similar behavior with shear stress rising to peak shear strength τ_p, and then decreasing to lower shear strength at large displacement. Interface failures occurred for all tests with $\sigma_n \leq 692$ kPa, except one specimen that experienced partial internal failure ($\sigma_n = 692$ kPa; $R = 100$ mm/min). For $\sigma_n = 1{,}382$ kPa, internal failure occurred for $R = 1$ mm/min, partial internal failures occurred for $R = 0.1$ and 100 mm/min, and interface failures occurred for $R \geq 10{,}000$ mm/min. For

$\sigma_n = 2{,}071$ kPa, internal failures occurred for $R \leq 1$ mm/min, partial internal failure occurred for $R = 100$ mm/ min, and interface failures occurred for $R \geq 10{,}000$ mm/min.

Stress-displacement relationships for $\sigma_n = 13$ kPa are presented in Fig. 2(a) and correspond to normal stress conditions typical of a landfill cover system. Shear strength reaches a peak at small displacements and then decreases to a residual value τ_r, which is nearly the same for each displacement rate. These relationships display oscillations with a consistent spacing of approximately 5 mm and a magnitude that increases with increasing displacement rate. The spacing of oscillations matches the spacing between GMX asperities and, because rows of asperities were aligned in the direction of shear for these tests, apparently indicates the effect of initial asperity imprints on the upper geotextile of the GCL during the second hydration stage. These imprints also apparently disappeared with time once shearing commenced, which explains the larger oscillation magnitudes for higher displacement rates. The effect of GMX texturing was confirmed by performing a replicate test with a smooth geomembrane (not shown), which indicated no such oscillations in the stress-displacement relationship (Ross 2009). At this low normal stress, there was little to the GMX or GCL and, as a result, no strength reduction after a displacement of approximately 50 mm.

Stress-displacement relationships for the higher normal stress levels are presented in Figs. 2(b–e). These relationships also indicate peak strengths at small displacements, followed by more gradual post-peak strength reduction. For the GMX/GCL interface failures, strength reduction occurred due to flattening of asperities and formation of shallow grooves in the upper geotextile of the GCL. Large-displacement shear strengths τ_{200}, measured at $\delta = 200$ mm, are not residual values for the interface failures. GCL internal failures exhibit larger post-peak strength reduction due to failure of the needle-punched reinforcement. Residual strength was not reached at $\sigma_n = 1{,}382$ kPa ($R = 1$ mm/min), but was reached for two tests at $\sigma_n = 2{,}071$ kPa ($R = 0.1$ and 1 mm/ min). Internal shear failures were well developed for these latter two tests and the stress-displacement relationships are clearly distinguished in Fig. 2(e). At constant normal stress, residual strengths for internal failures are lower than large-displacement strengths for interface failures due to the low shear strength of hydrated bentonite. GCL partial internal failures yielded stress-displacement relationships with features intermediate between those for interface and internal failures. Some relationships in Fig. 2 display a temporary stress peak at small displacements (<4 mm), which occurs as the GCL slips slightly on the truss plates before the teeth begin to mobilize the full strength of the specimen. The shear resistance associated with these peaks increases with increasing displacement rate and suggests a rapid shear effect for the lower geotextile against the truss plate gripping surface.

Volume Change Behavior

Corresponding relationships for volume change of the GMX/GCL composite liners are shown in Fig. 3. Values of vertical displacement indicate movement of the load plate and thus changes in specimen thickness, with negative values indicating contraction. Fig. 3(a) shows little volume change for interface failures at $\sigma_n = 13$ kPa, with contractive behavior for $R \leq 100$ mm/min and expansive behavior for $R \geq 10{,}000$ mm/min. Regular oscillations for some of these relationships are again consistent with the spacing between GMX asperities. Volume change data for interface failures at $\sigma_n = 348$ and 692 kPa and one partial internal failure at $\sigma_n = 692$ kPa are shown in Figs. 3(b and c). Specimen contraction was maximum for $R = 0.1$ mm/min and then decreased with increasing displacement rate. This is consistent with the trend of GCL water contents in Fig. 1 and reflects less time available for bentonite consolidation under the higher mean stress conditions imposed during shear. Volume change relationships for the highest normal stress levels, shown in Figs. 3(d and e), display a more complicated response due to different failure modes for these specimens. Interface failures at high displacement rates indicate relatively small volume change and a tendency for expansion associated with peak strength mobilization. At lower displacement rates, GCL internal failures and partial internal failures generally show contraction followed by expansion. Partial internal failures show the largest expansion due to typical wrinkling and/or overlap of the upper geotextile during shear.

Peak Shear Strength

Peak shear strengths are plotted versus displacement rate for each normal stress in Fig. 4. Some replicate tests were conducted to better define the measured trends and those data are also shown. Symbols indicate the failure mode for each specimen and dashed lines are used to connect points with different failure modes. Peak strength of the GMX/GCL specimens increased with increasing displacement rate at the lowest normal stress ($\sigma_n = 13$ kPa) and was approximately constant for each of the next two normal stress levels ($\sigma_n = 348$ and 692 kPa). One GCL partial internal failure at $\sigma_n = 692$ kPa follows the same trend. This is generally consistent with results reported by Triplett and Fox (2001) and McCartney et al. (2009) for GMX/GCL interfaces and Stark et al. (1996) for a GMX/NW GT interface, in which displacement rates in the quasi-static range had little effect on peak shear strength at low to intermediate normal stress. At $\sigma_n = 1{,}382$ kPa, peak strengths were similar for internal and partial internal failures ($R \leq 100$ mm/min), and then increased slightly for interface failures at high displacement rates ($R \geq 10{,}000$ mm/min). For $\sigma_n = 2{,}071$ kPa, internal failures at low displacement rates ($R \leq 1$ mm/ min) again yielded smaller peak strengths relative to interface failures at high displacement rates ($R \geq 10{,}000$ mm/ min); however, one partial internal failure at $R = 100$ mm/ min produced the largest peak strength.

The data in Fig. 4 indicate that failure mode of the GMX/GCL composite liners was dependent not only on normal stress, as previously reported (e.g., Eid 2011; Fox and Ross 2011), but also on displacement rate. GCL internal failures occurred at high normal stress and low displacement rate. As normal stress decreased or displacement rate increased, failure mode transitioned to the GMX/GCL interface. Fox et al. (2015) reported that GCL internal shear strength generally increases with increasing displacement rate, which explains the failure mode transition observed at higher normal stress levels in Fig. 4. The data also indicate that the standard displacement rate for static shear tests of GMX/GCL composite liners ($R = 1$ mm/min) yielded a conservative (i.e., low) value of peak shear strength for each normal stress.

Displacement at Peak Strength

Corresponding relationships for displacement at peak shear strength δ_p are presented in Fig. 5. Values generally increase with increasing normal stress, which is consistent with the findings of Hebeler et al. (2005) for a structured GMX/NW GT interface. Hebeler et al. (2005) attributed the effect to a change in controlling failure mechanism from surficial interaction without hook and loop strength at low normal stress to matrix-level interaction at higher normal stress. Interestingly, this trend is opposite to the behavior observed for GCL internal shear tests (Fox et al. 2015). In other

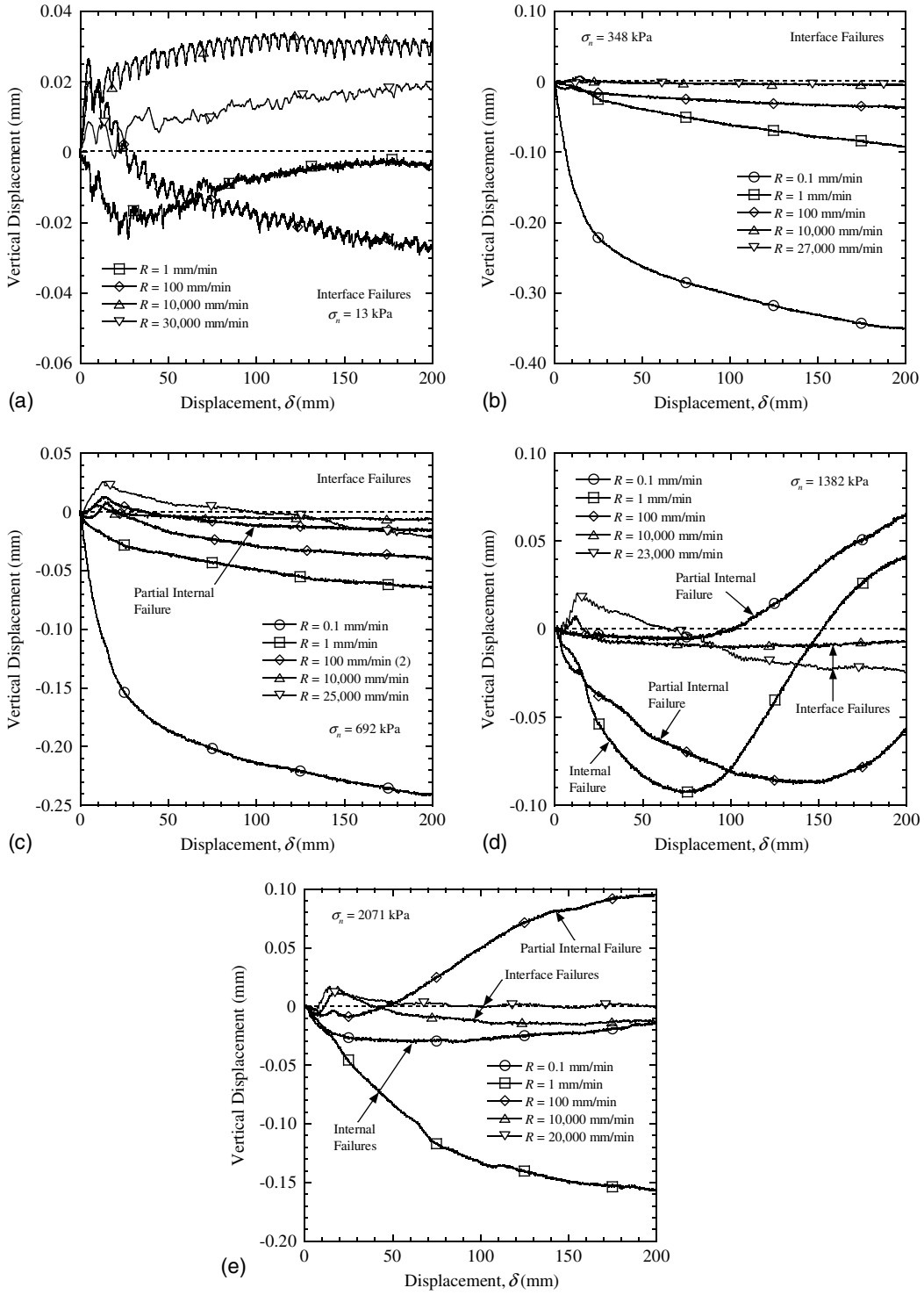

Fig. 3. Representative volume change-displacement relationships: (a) $\sigma_n = 13$ kPa; (b) $\sigma_n = 348$ kPa; (c) $\sigma_n = 692$ kPa; (d) $\sigma_n = 1{,}382$ kPa; (e) $\sigma_n = 2{,}071$ kPa

studies for GMX/GCL interfaces, Triplett and Fox (2001) reported that δ_p ranged from 7 to 21 mm and showed no clear trend with normal stress, whereas McCartney et al. (2009) and Bacas et al. (2011) reported an increase in δ_p with increasing normal stress.

At the lowest normal stress ($\sigma_n = 13$ kPa), values are relatively constant and range from 2.7 to 4.3 mm. At higher normal stress levels, Fig. 5 indicates that δ_p generally decreases with increasing displacement rate, ranging from 8 to 17 mm for $R \leq 10{,}000$ mm/min, and then decreases sharply to approximately 5 mm at the highest displacement rate ($R = R_{\max}$). This behavior does not appear to be significantly affected by failure mode and is consistent with a mechanism discussed by Ridruejo et al. (2011), in which lack of time for fiber rearrangement produces higher stiffness in nonwoven geotextiles with increasing strain rate. Absence of a similar trend at the lowest normal stress suggests that this mechanism is not important for predominantly surficial GMX/NW GT interactions.

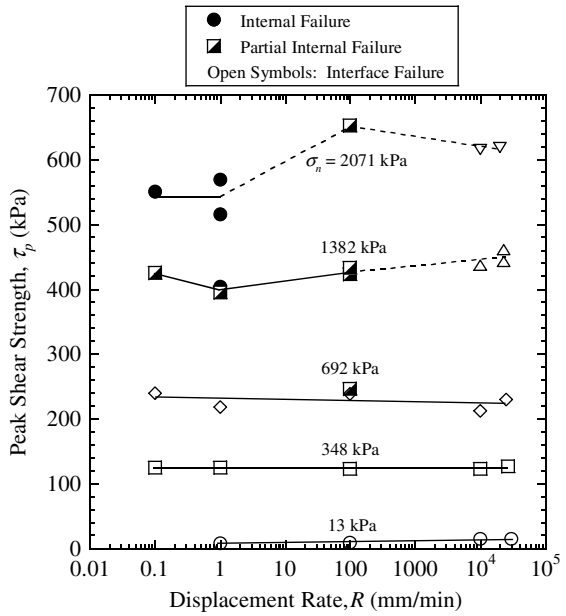

Fig. 4. Peak shear strengths

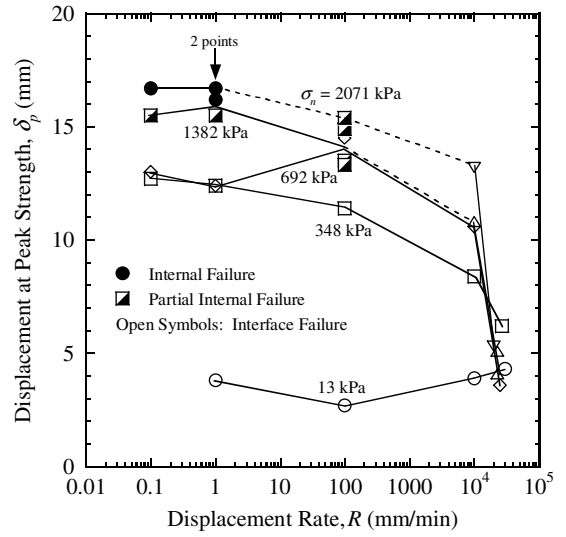

Fig. 5. Displacements at peak shear strength

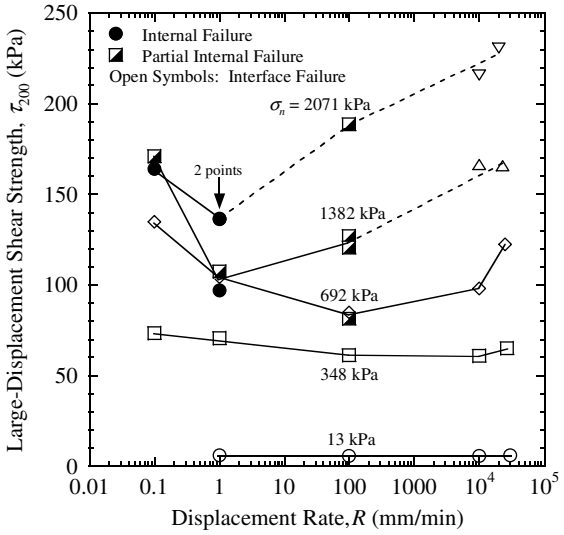

Fig. 6. Large-displacement shear strengths

Large-Displacement Shear Strength

Large-displacement shear strengths are presented in Fig. 6. Displacement rate had little effect for $\sigma_n = 13$ kPa, with τ_{200} values ranging from 5.6 to 6.1 kPa. This is in general agreement with the findings of Triplett and Fox (2001) for interface failures of similar materials at low normal stress. Large-displacement strengths for $\sigma_n = 348$ kPa are also approximately constant; however, these values decrease and then increase slightly with increasing displacement rate. For $\sigma_n = 692$ kPa, this trend becomes distinct, with a minimum value at $R = 100$ mm/min, and is not related to failure mode. A reasonable explanation involves the combined effects of positive excess pore pressures and rapid shearing at the GMX/GCL interface. For $R \leq 100$ mm/min, volume change behavior in Fig. 3(c) suggests that excess pore pressures will increase with increasing displacement rate and thus reduce large-displacement strengths. For $R > 100$ mm/min, excess pore pressures are likely to be approximately constant; however, rapid shearing effects such as increasing GT and GMX asperity stiffness with increasing displacement rate yield higher values of large-displacement strength.

Large-displacement shear strengths measured for $\sigma_n = 1{,}382$ and 2,071 kPa show similar behavior, with minimum values at $R = 1$ mm/min, and include effects of changing failure mode. Relative to interface failures at higher displacement rates, partial to complete GCL internal failures yielded smaller values of τ_{200} due to the low strength of hydrated bentonite. These effects can be important as indicated for $\sigma_n = 2{,}071$ kPa, where the minimum value of τ_{200} (136 kPa) is 41% lower than the maximum value (231 kPa) at $R = 20{,}000$ mm/min. The significant effect of failure mode is also observed for $R = 0.1$ mm/min, where large-displacement strengths measured for a partial internal failure at $\sigma_n = 1{,}382$ and an internal failure at $\sigma_n = 2{,}071$ kPa are essentially the same. At the highest stress level, the decrease of GCL internal residual strength between $R = 0.1$ and 1 mm/min likely results from shear-induced excess pore pressures and is consistent with the findings of Fox et al. (2015). The data of Fig. 6 indicate that the standard displacement rate for static shear tests of GMX/GCL composite liners ($R = 1$ mm/min) yielded unconservative values of large-displacement shear strength for some normal stress conditions.

Shear Strength Envelopes

Peak shear strengths are plotted versus normal stress for each displacement rate in Fig. 7(a). In general, the points fall close together and show consistent trends. For clarity, strength envelopes are drawn only for the standard static displacement rate ($R = 1$ mm/min) and the maximum displacement rate ($R = R_{\max}$). Tangent friction angles decrease gradually with increasing normal stress and render each envelope slightly concave-down. Using only the endpoints at $\sigma_n = 13$ and 2,071 kPa, linear (i.e., conservative) envelopes for peak shear strength are defined as

$$\tau_p = 4.5 \text{ kPa} + \sigma_n \tan 14.5° R = 1 \text{ mm/min} \quad (1)$$

$$\tau_p = 10.9 \text{ kPa} + \sigma_n \tan 16.3° R = R_{\max} \quad (2)$$

where calculated strength parameters correspond to total normal stresses. Eqs. (1) and (2) indicate that cohesion intercept and friction

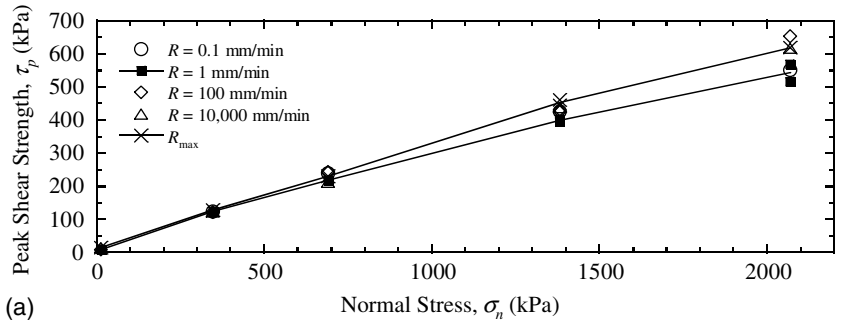

(a)

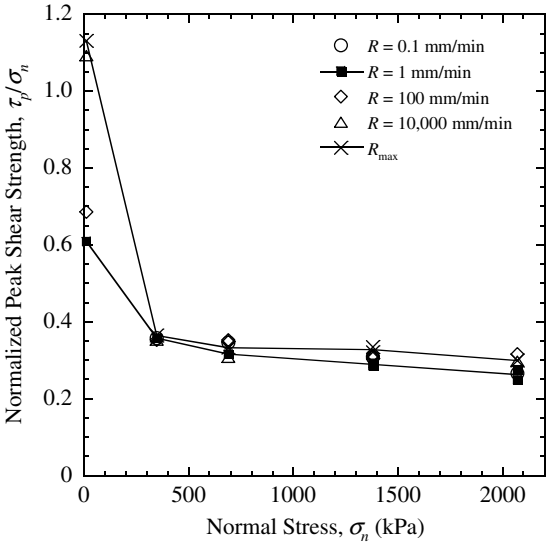

(b)

Fig. 7. Strength envelopes: (a) peak shear strength; (b) normalized peak shear strength

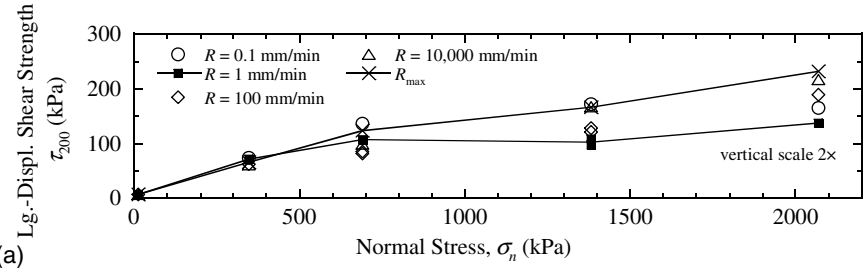

(a)

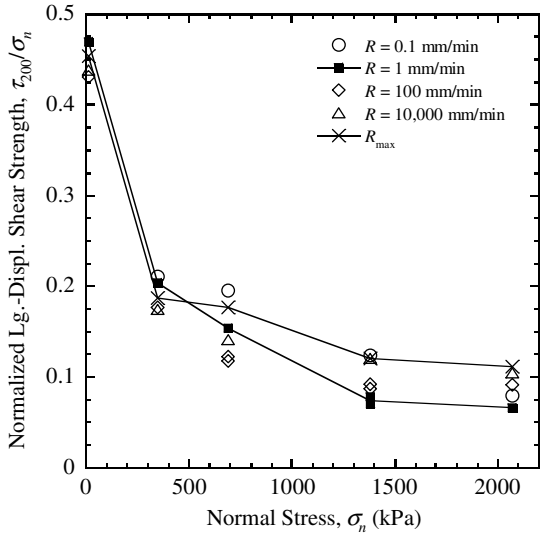

(b)

Fig. 8. Strength envelopes: (a) large-displacement shear strength; (b) normalized large-displacement shear strength

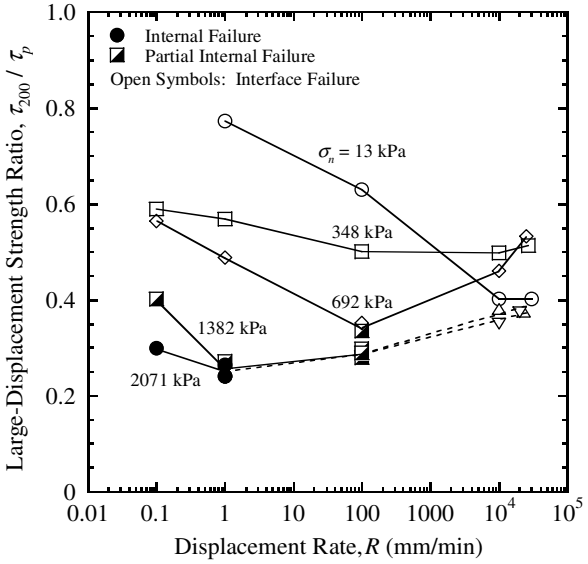

Fig. 9. Large-displacement strength ratios

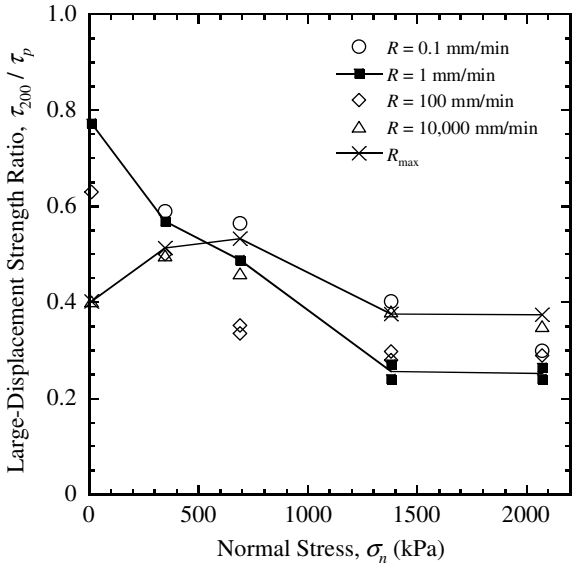

Fig. 10. Effect of normal stress on large-displacement strength ratio

angle increase with increasing displacement rate. Corresponding values of normalized peak shear strength τ_p/σ_n are shown in Fig. 7(b) and decrease with increasing normal stress. Fig. 7 confirms that the static strength envelope ($R = 1$ mm/min) yields conservative values of peak shear strength for this GMX/GCL composite liner.

Large-displacement shear strengths and envelopes for the same displacement rates are shown in Fig. 8(a). The static strength envelope ($R = 1$ mm/min) indicates the effect of changing failure mode with increasing normal stress. For $\sigma_n \leq 692$ kPa, interface failures yield large-displacement strengths that increase nonlinearly with increasing normal stress. The envelope decreases slightly between $\sigma_n = 692$ and 1,382 kPa as the failure mode changes from interface to internal shear, and then increases again to $\sigma_n =$ 2,071 kPa. At $\sigma_n = 2{,}071$ kPa, the secant friction angle for $R =$ 0.1 mm/min is 4.6° and in close agreement with the corresponding value of 4.7° measured by Fox and Ross (2011) for internal shear of the same GCL product. The secant friction angle for $R = 1$ mm/min is 3.8°, which is significantly lower and underscores the importance of displacement rate for these tests. Fig. 8(a) confirms that displacement rate had little effect on large-displacement shear strengths for the two lowest normal stress levels. For $\sigma_n \geq 692$ kPa, the R_{max} envelope deviates from the static envelope and indicates substantially higher large-displacement strengths associated with GMX/GCL interface failures. Corresponding values of normalized large-displacement shear strength τ_{200}/σ_n are shown in Fig. 8(b) and decrease with increasing normal stress for each displacement rate.

Large-Displacement Strength Ratio

Large-displacement strength ratios τ_{200}/τ_p are presented in Fig. 9. Values range from 0.24 to 0.77 and show wide variability at low displacement rates, due to changing specimen failure mode. The lowest values correspond to GCL internal failure and the residual strength of hydrated bentonite. For higher displacement rates, all failures occurred at the GMX/GCL interface and values converge to a range of 0.35–0.55. The same data are plotted in Fig. 10 and, in general, indicate larger post-peak strength reduction with increasing normal stress. This is consistent with the findings of Fox and Ross (2011) for GMX/GCL static shear tests, and opposite to the behavior observed for corresponding GCL internal shear tests (Fox et al. 2015). At high displacement rates, the data for $\sigma_n \leq 692$ kPa display a reverse (i.e., increasing) trend. Figs. 9 and 10 indicate that the GMX/GCL composite liner experienced significant post-peak strength reduction for all conditions, including high displacement rates and normal stress levels, with magnitude strongly influenced by failure mode.

Conclusions

The following conclusions are based on the foregoing experimental investigation of the dynamic shear strength of a composite liner consisting of a high-density polyethylene (HDPE) textured geomembrane (GMX) over a hydrated nonwoven/nonwoven needle-punched geosynthetic clay liner (GCL) for displacement-controlled monotonic (i.e., single direction) loading conditions:

1. Large-scale direct shear tests were conducted for five normal stress σ_n levels ranging from 13 to 2,071 kPa and five shear displacement rates R ranging from 0.1 to 30,000 mm/min. Shear stress-displacement relationships indicate well-defined peak shear strengths, followed by post-peak strength reduction to lower large-displacement shear strengths.
2. Failure mode for the GMX/GCL composite liner was dependent on both normal stress and displacement rate. GCL internal failures occurred at high normal stress and low displacement rate. As normal stress decreased or displacement rate increased, failure mode transitioned to the GMX/GCL interface.
3. Peak shear strengths τ_p increased with increasing displacement rate for the lowest normal stress ($\sigma_n = 13$ kPa) and were approximately constant for each of the next two normal stress levels ($\sigma_n = 348$ and 692 kPa). At higher normal stress, internal failures at low displacement rates generally yielded smaller peak strengths than interface failures at high displacement rates. Displacements at peak shear strength increased with increasing normal stress and, for $\sigma_n \geq 348$ kPa, decreased with increasing displacement rate.
4. Large-displacement shear strengths τ_{200} were approximately constant for each of the two lowest normal stress levels ($\sigma_n = 13$ and 348 kPa). For $\sigma_n \geq 692$ kPa, large-displacement

strengths decreased and then increased with increasing displacement rate. This is attributed primarily to changing failure mode for $\sigma_n = 1{,}382$ and 2,071 kPa, but was also observed for interface failures at $\sigma_n = 692$ kPa. Large-displacement strength ratios τ_{200}/τ_p ranged from 0.24 to 0.77, with lower values corresponding to GCL internal failures, and indicate significant post-peak strength reduction for all test conditions.

5. Peak strength envelopes are slightly nonlinear (concave-down) and show dependence on displacement rate at higher normal stress. Linear envelopes drawn through the end points indicate that peak strength parameters (cohesion intercept, friction angle) increase slightly with increasing displacement rate. Large-displacement strength envelopes show greater dependence on displacement rate at higher normal stress due to the effect of changing failure mode.
6. The standard displacement rate for static shear tests of GMX/GCL composite liners ($R = 1$ mm/min) yielded conservative values of peak shear strength but unconservative values of large-displacement shear strength for some normal stress conditions.

Acknowledgments

Financial support for this investigation was provided by Grant No. CMMI-0800030 from the Geotechnical Engineering Program of the U.S. National Science Foundation and a grant from CETCO of Hoffman Estates, Illinois. Geomembrane materials were provided by Agru America of Georgetown, South Carolina, and GCL materials were provided by CETCO. This support is gratefully acknowledged. The writers thank Alexander Stern for assistance with some of the experimental work, and Jim Olsta of CETCO for support of this research.

References

ASTM. (2009). "Standard test method for determining average bonding peel strength between the top and bottom layers of needle-punched geosynthetic clay liners." *D6496*, West Conshohocken, PA.

ASTM. (2010a). "Standard test method for determining tensile properties of nonreinforced polyethylene and nonreinforced flexible polypropylene geomembranes." *D6693*, West Conshohocken, PA.

ASTM. (2010b). "Standard test method for measuring core thickness of textured geomembrane." *D5994*, West Conshohocken, PA.

ASTM. (2013a). "Standard test method for determining the internal and interface shear resistance of geosynthetic clay liner by the direct shear method." *D6243*, West Conshohocken, PA.

ASTM. (2013b). "Standard test method for index puncture resistance of geomembranes and related products." *D4833*, West Conshohocken, PA.

ASTM. (2013c). "Standard test method for tear resistance (graves tear) of plastic film and sheeting." *D1004*, West Conshohocken, PA.

ASTM. (2013d). "Standard test methods for density and specific gravity (relative density) of plastics by displacement." *D792*, West Conshohocken, PA.

ASTM. (2014). "Standard test method for linear dimensional changes of nonrigid thermoplastic sheeting or film at elevated temperature." *D1204*, West Conshohocken, PA.

Bacas, B. M., Konietzky, H., Berini, J. C., and Sagaseta, C. (2011). "A new constitutive model for textured geomembrane/geotextile interfaces." *Geotext. Geomembr.*, 29(2), 137–148.

Byrne, R. J. (1994). "Design issues with strain-softening interfaces in landfill liners." *Proc., Waste Tech '94*, Charleston, SC, 1–26.

Chen, Y.-M., Lin, W.-A., and Zhan, T. L. T. (2010). "Investigation of mechanisms of bentonite extrusion from GCL and related effects on the shear strength of GCL/GM interfaces." *Geotext. Geomembr.*, 28(1), 63–71.

Chiu, P., and Fox, P. J. (2004). "Internal and interface shear strengths of unreinforced and needle-punched geosynthetic clay liners." *Geosynthetics Int.*, 11(3), 176–199.

Daniel, D. E., Koerner, R. M., Bonaparte, R., Landreth, R. E., Carson, D. A., and Scranton, H. B. (1998). "Slope stability of geosynthetic clay liner test plots." *J. Geotech. Geoenviron. Eng.*, 10.1061/(ASCE)1090-0241(1998)124:7(628), 628–637.

Eid, H. T. (2011). "Shear strength of geosynthetic composite systems for design of landfill liner and cover slopes." *Geotext. Geomembr.*, 29(3), 335–344.

Fox, P. J., and Kim, R. H. (2008). "Effect of progressive failure on measured shear strength of geomembrane/GCL interface." *J. Geotech. Geoenviron. Eng.*, 10.1061/(ASCE)1090-0241(2008)134:4(459), 459–469.

Fox, P. J., Nye, C. J., Morrison, T. C., Hunter, J. G., and Olsta, J. T. (2006). "Large dynamic direct shear machine for geosynthetic clay liners." *Geotech. Test. J.*, 29(5), 392–400.

Fox, P. J., and Ross, J. D. (2011). "Relationship between NP GCL internal and HDPE GMX/NP GCL interface shear strengths." *J. Geotech. Geoenviron. Eng.*, 10.1061/(ASCE)GT.1943-5606.0000490, 743–753.

Fox, P. J., Rowland, M. G., and Scheithe, J. R. (1998). "Internal shear strength of three geosynthetic clay liners." *J. Geotech. Geoenviron. Eng.*, 10.1061/(ASCE)1090-0241(1998)124:10(933), 933–944.

Fox, P. J., and Stark, T. D. (2004). "State-of-the-art report: GCL shear strength and its measurement." *Geosynthetics Int.*, 11(3), 141–175.

Fox, P. J., Sura, J. M., and Nye, C. J. (2015). "Dynamic shear strength of a needle-punched GCL for monotonic loading." *J. Geotech. Geoenviron. Eng.*, 04015025.

Gilbert, R. B., Fernandez, F., and Horsfield, D. W. (1996). "Shear strength of reinforced geosynthetic clay liner." *J. Geotech. Eng.*, 10.1061/(ASCE)0733-9410(1996)122:4(259), 259–266.

Hebeler, G. L., Frost, J. D., and Myers, A. T. (2005). "Quantifying hook and loop interaction in textured geomembrane—Geotextile systems." *Geotext. Geomembr.*, 23(1), 77–105.

Kim, J., Riemer, M., and Bray, J. D. (2005). "Dynamic properties of geosynthetic interfaces." *Geotech. Test. J.*, 28(3), 1–9.

Lai, J., Daniel, D. E., and Wright, S. G. (1998). "Effects of cyclic loading on internal shear strength of unreinforced geosynthetic clay liner." *J. Geotech. Geoenviron. Eng.*, 10.1061/(ASCE)1090-0241(1998)124:1(45), 45–52.

Lo Grasso, S. A., Massimino, M. R., and Maugeri, M. (2002). "Dynamic analysis of geosynthetic interfaces by shaking table tests." *7th Int. Conf. on Geosynthetics*, Vol. 4, A.A. Balkema, Lisse, 1335–1338.

McCartney, J. S., Zornberg, J. G., and Swan, R. H., Jr. (2002). "Internal and interface shear strength of geosynthetic clay liners (GCLs)." *Geotech. Res. Rep.*, Dept. of Civil, Environmental and Architectural Engineering, Univ. of Colorado, Boulder, CO, 450.

McCartney, J. S., Zornberg, J. G., and Swan, R. H., Jr. (2009). "Analysis of a large database of GCL-geomembrane interface shear strength results." *J. Geotech. Geoenviron. Eng.*, 10.1061/(ASCE)1090-0241(2009)135:2(209), 209–223.

Nye, C. J., and Fox, P. J. (2007). "Dynamic shear behavior of a needle-punched geosynthetic clay liner." *J. Geotech. Geoenviron. Eng.*, 10.1061/(ASCE)1090-0241(2007)133:8(973), 973–983.

Park, I. J., Seo, M. W., Park, J. B., Kwon, S. Y., and Lee, J. S. (2004). "Estimation of the dynamic properties for geosynthetic interfaces." *Paper No. 3210, 13th World Conf. on Earthquake Engineering*, Vancouver, BC, Canada.

Ridruejo, A., Gonzalez, C., and LLorca, J. (2011). "Micromechanisms of deformation and fracture of polypropylene nonwoven fabrics." *Int. J. Solids Struct.*, 48(1), 153–162.

Ross, J. D. (2009). "Static and dynamic shear strength of a geomembrane/geosynthetic clay liner interface." M.S. thesis, Dept. of Civil and Environmental Engineering and Geodetic Science, Ohio State Univ., Columbus, OH.

Ross, J. D., Fox, P. J., and Olsta, J. T. (2010). "Dynamic shear testing of a geomembrane/geosynthetic clay liner interface." *9th Int. Conf. on Geosynthetics*, IGS, Guaruja, Brazil.

Stark, T. D., and Eid, H. T. (1996). "Shear behavior of reinforced geosynthetic clay liners." *Geosynthetics Int.*, 3(6), 771–786.

Stark, T. D., Williamson, T. A., and Eid, H. T. (1996). "HDPE geomembrane/geotextile interface shear strength." *J. Geotech. Eng.*, 10.1061/(ASCE)0733-9410(1996)122:3(197), 197–203.

Thielmann, S. S., Fox, P. J., and Athanassopoulos, C. (2013). "Interface shear testing of GCL liner systems for very high normal stress conditions." *Stability and Performance of Slopes and Embankments III, GSP No. 231*, ASCE, Reston, VA, 63–71.

Triplett, E. J., and Fox, P. J. (2001). "Shear strength of HDPE geomembrane/geosynthetic clay liner interfaces." *J. Geotech. Geoenviron. Eng.*, 10.1061/(ASCE)1090-0241(2001)127:6(543), 543–552.

Vukelic, A., Szavits-Nossan, A., and Kvasnicka, P. (2008). "The influence of bentonite extrusion on shear strength of GCL/geomembrane interface." *Geotext. Geomembr.*, 26(1), 82–90.